The Fermi surface of Sn/Ge(111) and Pb/Ge(111)

2007 J. Phys.: Condens. Matter 19 355008

(http://iopscience.iop.org/0953-8984/19/35/355008)

IOP PUBLISHING JOURNAL OF PHYSICS: CONDENSED MATTER

J. Phys.: Condens. Matter **19** (2007) 355008 (18pp) doi:10.1088/0953-8984/19/35/355008

The Fermi surface of Sn/Ge(111) and Pb/Ge(111)

A Tejeda[1], R Cortés[2], J Lobo[3], E G Michel[4] and A Mascaraque[2,5]

[1] Matériaux et Phénomènes Quantiques, UMR CNRS 7162, Université Paris Diderot, 75205 Paris, France
[2] Departamento de Física de Materiales, Universidad Complutense de Madrid, 28040 Madrid, Spain
[3] Physik-Institut, University of Zurich and Swiss Light Source, Paul Scherrer Institut, Switzerland
[4] Departamento de Física de la Materia Condensada, Universidad Autónoma de Madrid, 28049 Madrid, Spain

E-mail: arantzazu.mascaraque@fis.ucm.es

Received 15 March 2007, in final form 23 May 2007
Published 20 August 2007
Online at stacks.iop.org/JPhysCM/19/355008

Abstract

The analysis of the electronic structure and Fermi surface of 0.33 monolayers (ML) of Sn/Ge(111) and Pb/Ge(111) has played an important role in understanding the phase transition from a room-temperature $(\sqrt{3} \times \sqrt{3})$R30° reconstruction to a (3×3) reconstruction below ∼200 K. Nowadays, the increasing resolution of image-type electron analysers enables us to obtain whole sets of constant-energy surfaces and energy-distribution curves. We review the electronic structure of Sn and Pb on Ge(111) and report high-resolution angle-resolved photoemission data for Sn/Ge(111)-(3×3) at 110 K. The results exclude nesting or any opening of a gap in the (3×3) phase at this temperature. From a comparison with density functional theoretical calculations, we conclude that the results on the electronic structure are only compatible with a (3×3) unit cell with one Sn atom displaced upward from the other two.

(Some figures in this article are in colour only in the electronic version)

1. Introduction

Low-dimensional materials exhibit a wide range of phenomena that are either modified, enhanced or unexpected for their three-dimensional (3D) analogues. Conspicuous examples are two-dimensional (2D) phase transitions [1], including 2D superconductivity [2], metal–insulator phase transitions [3], stabilization of 2D charge density waves [4–6] or 2D ferroelectricity [7], among others. Due to this fact, great effort has been devoted over the last few decades to both theoretical and experimental studies of phase transitions at surfaces. In

[5] Author to whom any correspondence should be addressed.

this review, we will concentrate in the case of 0.33 monolayers (ML) of Sn or Pb adsorbed on Ge(111): two interfaces which have deserved ample attention since the discovery of a surface phase transition from a room-temperature (RT) ($\sqrt{3} \times \sqrt{3}$)R30° phase to a (3×3) phase below ∼200 K [8, 9]. Several different mechanisms have been put forward to explain this phase transition, such as nesting instabilities [8], electron correlation effects [8, 9], defect-mediated density waves [10–12], and dynamical fluctuations [13]. In all the cases, it is clear that the electronic structure in the region near the Fermi energy should play a crucial role, and thus detailed knowledge of the Fermi surface is of critical importance to understand the properties of these interfaces under debate. Although the structure of Pb or Sn on Si(111) and on Ge(111) is apparently the same for 0.33 ML coverage, the reconstructions on Si(111) exhibit specific features. For instance, Sn/Si(111) does not show any structural transition down to 6 K [14, 15]. In the case of Pb/Si(111), there is a phase transition [16], but the domains are relatively small, and it is observed only by scanning tunelling microscopy (STM) [17, 18]. For this reason, the particular cases of Pb/Si(111) and Sn/Si(111) will not be considered in this review.

The deposition of 0.33 ML of either Pb or Sn on Ge(111), followed by a slight anneal to enhance the surface ordering, gives rise at RT to the formation of a phase with ($\sqrt{3} \times \sqrt{3}$)R30° symmetry [19–21] (RT-$\sqrt{3}$ in order to distinguish it from another phase with $\sqrt{3}$ symmetry that appears at ∼25 K [22]; also see below). The $\sqrt{3}$ is a common reconstruction in metal/semiconductor interfaces [23, 24]. It is stabilized by the minimization of Ge dangling bonds: the adsorbate deposition reduces the number of dangling bonds from three to one when a single Sn or Pb atom per $\sqrt{3}$ unit cell occupies a T_4 site (i.e. the threefold-hollow site directly above second-layer Ge atoms). There is one adsorbate atom per $\sqrt{3}$ unit cell. In the case of Sn/Ge(111) and Pb/Ge(111), the RT-$\sqrt{3}$ phase exhibits a temperature-induced phase transition to a low-temperature (LT) phase of (3×3) symmetry [13, 25]. The (3×3) phase contains three adsorbate atoms per unit cell, still positioned on T_4 sites. Topographic STM images [8, 12, 22], together with theoretical calculations [26], consistently demonstrate that the (3×3) periodicity is observed, because one out of the three Sn or Pb atoms in the unit cell is displaced upward with respect to the other two (figures 1(b), (c)). At RT all three atoms appear equivalent in STM images [8], giving rise to the $\sqrt{3}$ symmetry (figure 2).

The first model proposed to explain the phase transition in Pb/Ge(111) was the stabilization of a surface charge density wave (CDW) [8]. The RT-$\sqrt{3}$ phase would evolve into a (3×3) phase induced by the stabilization of a surface CDW. It was claimed that the CDW instability was triggered by Fermi surface nesting and the opening of an electron correlation gap in the case of Pb/Ge(111) [8], or by electron correlation alone in the case of Sn/Ge(111) [9]. Electron correlation effects are expected to be significant in these interfaces, because the nearest-neighbour distance for the $\sqrt{3}$ structure on Ge(111) is ∼7 Å [27, 28]. However, models based on Fermi surface nesting were soon ruled out, as the experimental Fermi surface of the RT-$\sqrt{3}$ phase of Pb/Ge(111) was shown to exhibit no significant nesting [25]. Furthermore, angle-resolved photoemission experiments found that both phases are indeed metallic [25]. On the other hand, a detailed analysis of the electronic structure (Sn 4d core level and valence band) showed no significant differences between the RT-$\sqrt{3}$ and the (3×3) phases, suggesting that both phases should be similar from the structural point of view [29], and that the phase transition should be of the order–disorder type [13]. These experiments were interpreted in the light of molecular dynamic simulations and *ab initio* theoretical calculations [13, 30]. The ground state was found to be a metallic (3×3) structure. Its theoretical electronic band structure is shown in figure 1(d) [30]. There are two surface bands, one half-filled and one completely filled. These two bands are closely related to the charge transfer from the lower Sn atoms to the higher Sn atoms, as illustrated in figure 1(c) (see also section 2). As the temperature increases, there is a rapid fluctuation between Sn atoms at higher and lower positions, so that

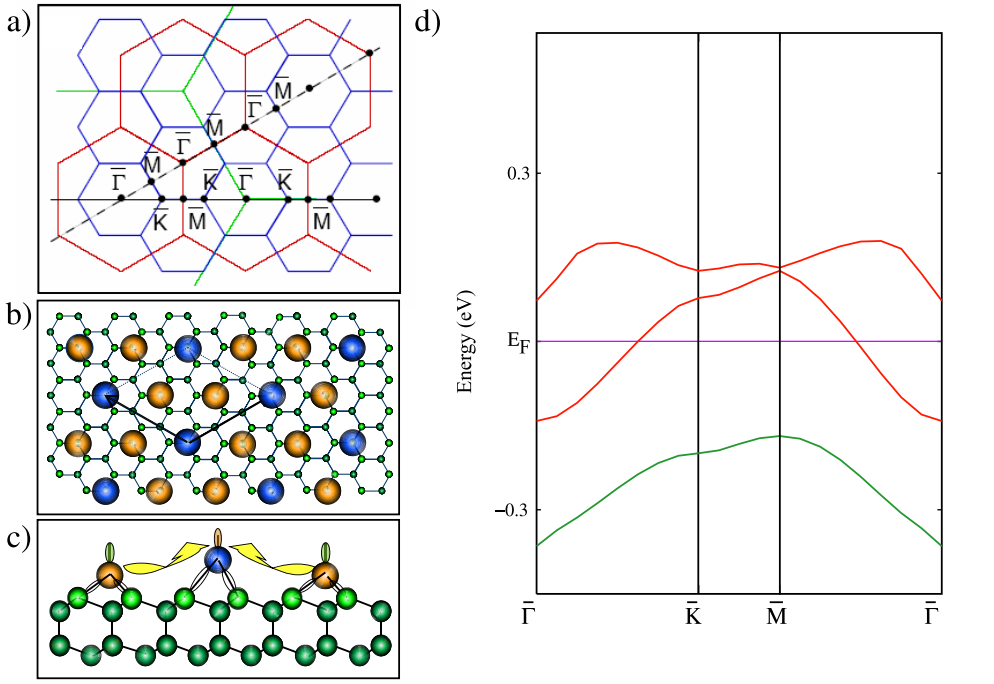

Figure 1. The (3 × 3) phase. (a) Surface Brillouin zones of the (1 × 1) (green, large hexagons), $\sqrt{3}$ (red, intermediate hexagons), (3 × 3) (blue, small hexagons) structures. (b) Top view of the real space. Small circles correspond to Ge atoms of the last bilayer. Large circles atoms are Sn–Pb atoms in T_4 symmetry sites. Blue (dark) and yellow (grey) circles correspond to inequivalent atoms in the LT (3 × 3) phase. (c) Side view of the real space, indicating charge transfer from the bottom Sn–Pb atoms to the upper ones (model 1U2D). (d) LDA theoretical band structure of the (3 × 3) phase within the 1U2D model (from [29]; see text for details).

the (3 × 3) long-range order is lost. A local (3 × 3) order survives up to temperatures above RT. The dynamical fluctuations model has been supported by evidence from several different sources [31–34], and the RT-$\sqrt{3}$ phase is currently described as a mixture of rapidly fluctuating, local (3 × 3) configurations, without long-range order [13, 25, 35–37].

The possible role of defects in the phase transition has also been analysed in detail. It was claimed that defects could mediate the formation of the (3 × 3) phase, and also that defect ordering was behind the phase transition [10–12]. Defects in the Sn layer are mainly Ge substitutional atoms, which pin locally (3 × 3) patches [12]. The defect concentration is in the range of 2–5% in Sn/Ge(111) but it is probably larger for Pb/Ge(111), depending on the preparation procedure [25]. Evidence from several different sources has shown that defect ordering is not the main driving force of the phase transition: first, theoretical calculations show that the defect–defect interaction is very localized [38], so it cannot order defects at low temperature. Second, STM studies on Pb/Si(111) have conclusively shown that the phase transition also takes place in defect-free areas, without any defect movement [18]. The role of the existing defects in the phase transition has been analysed using a Landau-like approach in [39, 40]. From this evidence, it is clear that the Fermi surface shape is not affected by the presence of defects in the surface and that defect interaction is not the mechanism driving the phase transition.

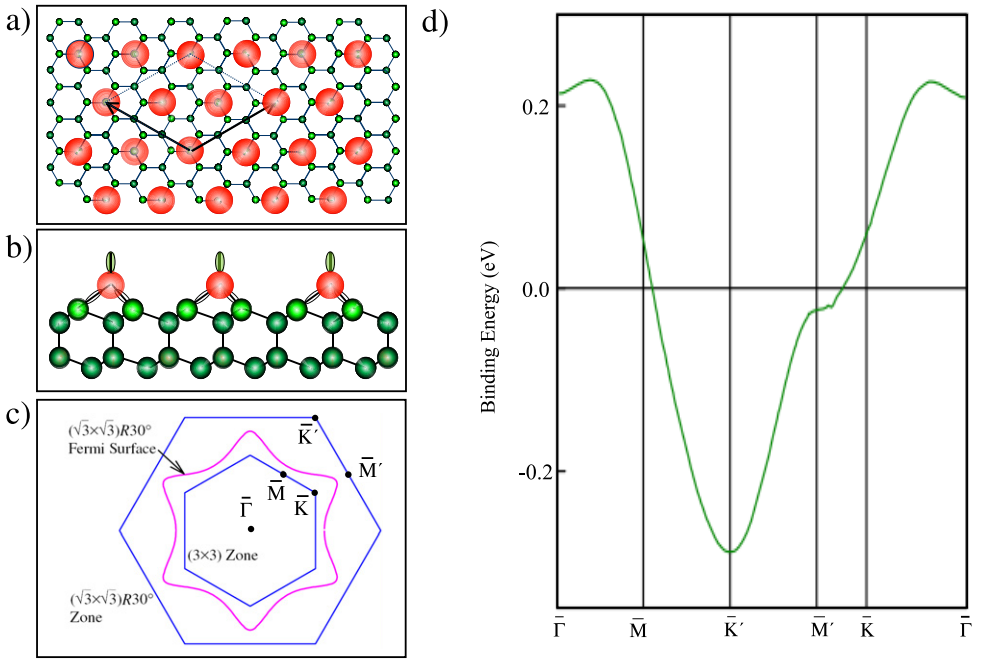

Figure 2. The hypothetical flat and metallic ($\sqrt{3} \times \sqrt{3}$)R30° phase. (a) Top view of real space. Small circles correspond to Ge atoms of the last bilayer. Large circles are Sn–Pb atoms in T_4 symmetry sites. (b) Side view of the real space. All adsorbate atoms are at the same height and there is no charge transfer between Sn–Pb atoms. (c) Calculated Fermi surface for a flat metallic Sn/Ge(111)-($\sqrt{3} \times \sqrt{3}$)R30° surface (from [51]. The Fermi surface of the analogous Pb/Ge(111) phase has the same shape, with a slightly smaller size, so that there is nesting in $\overline{\mathrm{M}}$ points (see [9]). (d) LDA theoretical band structure for a flat metallic ($\sqrt{3} \times \sqrt{3}$)R30°-Sn/Ge(111) surface (from [51]).

At lower temperatures, another phase transition has recently been found for both Sn/Ge(111) (∼25 K) [22] and Pb/Ge(111) (∼76 K) [41]. In the case of Sn/Ge(111), the (3 × 3) reconstruction undergoes a fully reversible temperature-induced phase transition at ∼25 K into another phase of $\sqrt{3}$ symmetry (LT-$\sqrt{3}$). The vertical distortion of the (3 × 3) phase disappears in the LT-$\sqrt{3}$ phase and all Sn atoms become equivalent. Concomitantly with the structural phase transition, a band gap opens along the whole reciprocal space. The phase transition is interpreted as the formation of a Mott insulator for a narrow half-filled band in a two-dimensional triangular lattice [22, 42], which evidences the importance of electron correlation effects in this interface. The behaviour of Pb/Ge(111) is still subject to controversy. An early study found a new phase transition, which reverts the well-ordered (3 × 3) phase to a disordered phase at low temperature [41]. In the new phase, Pb atoms appear distorted, without apparent long-range order, generating an irregular structure, which has been described as glass-like. The distortion was explained in terms of competition between different interactions in a highly correlated electron system. However, other STM experiments cast doubt on this phase transition. Although filled-state STM images display the glassy phase, empty-state images still show the (3 × 3) reconstruction [43].

In this work, we review the studies of the electronic structure of Sn and Pb adsorbates on Ge(111). We will pay special attention to the Fermi energy region, whose analysis has been of particular relevance to claiming the presence of charge density waves, electronic correlations

or metal–insulator transitions in these systems. Recent improvement in electron analysers has enabled an increase in both the energy resolution and the energy window around the Fermi surface, for a given measuring time. As we will show in this article for Sn/Ge(111), when the electronic surface bands are measured with state-of-the-art resolution and image-type analysers, a deep understanding of the topology of the Fermi surface is made possible, which in turn allows us to confirm the most accepted mechanism for the phase transition and to discern clearly the correct atomic structure of the (3×3) reconstruction.

2. The electronic structure of Sn–Pb/Ge(111)

2.1. Pb/Ge(111)

In order to better understand the behaviour of these interfaces, it is very useful to consider first the electronic structure of a flat $\sqrt{3}$ structure. It is important to point out that this structure does not exist at RT (also see below), neither for Sn/Ge(111) nor for Pb/Ge(111), because the observed RT-$\sqrt{3}$ phase is due to a mixture of local (3×3) configurations. However, it is interesting to analyse how the bands of this *hypothetical*, flat $\sqrt{3}$ phase would be, and it also helps to understand the origin of the surface bands observed in the (3×3) phase. By analogy to metal/Si(111)-$\sqrt{3}$ reconstructions [23, 24, 44], we expect to observe two different surface state bands for a flat $\sqrt{3}$ phase. Each Pb atom has four valence band electrons, and binds to three substrate Ge atoms, through covalent bonding to the half-filled dangling bond of each (figures 2(a), (b)). The deepest (occupied) surface state band is related to Pb p_x and p_y states. A second surface band closer to the Fermi energy should be observed due to Pb p_z orbitals [44–47]. Simple electron counting shows that the p_z surface band is half-filled, and thus it should cross the Fermi energy, and the flat $\sqrt{3}$ phase should be metallic (figure 2(c)). Obviously, these arguments do not take into account possible electron correlation effects [28]. Early angle-resolved photoemission results [48] found two occupied surface bands, one of them very close to the Fermi energy, and a semiconducting surface. Taking into account the expected metallic behaviour, this was taken as an evidence of electron correlation effects in Pb/Ge(111). Later photoemission experiments [25] demonstrated that the lack of Fermi crossing that was found was due to an inadequate surface preparation, which may give rise to intermixing [45, 49], lack of long-range order [45, 50] and non-dispersive states with apparent semiconducting behaviour.

High-quality Pb/Ge(111) interfaces exhibit much different behaviour. The top surface band related to p_z orbitals appears split in two dispersing states [25], at variance with the prediction of a single band near the Fermi energy for a flat $\sqrt{3}$ phase. This electronic structure near the Fermi energy (i.e. two dispersive bands) is also observed in Sn/Ge(111) [13, 29], as described in detail in the next section. Figure 3 shows selected angle-resolved photoemission spectra along the $\overline{\Gamma K}$ high-symmetry direction of the RT-$\sqrt{3}$ surface Brillouin zone for Pb/Ge(111). The lowest binding energy (BE) surface band crosses the Fermi energy at the $\overline{M}$ point of the (3×3) phase [25] (see figure 1(a) for a scheme of the reciprocal lattice). The Fermi level crossing renders the surface metallic, in agreement with simple electron counting. But the most interesting result is that, upon cooling and crossing the phase transition, the electronic structure does not show any important change. The surface remains metallic for the (3×3) phase, with a quite similar band structure. The only remarkable change is that the upper surface state *S* is much more clearly split into two bands (S_1 and S_2) in the LT phase [25], as is clearly seen in figure 3. As mentioned above, the splitting is already observed at RT, because the peak is broad and asymmetric for all emission angles, and its rounded shape indicates the presence of two different surface bands close in binding energy. These two surface bands become resolved in

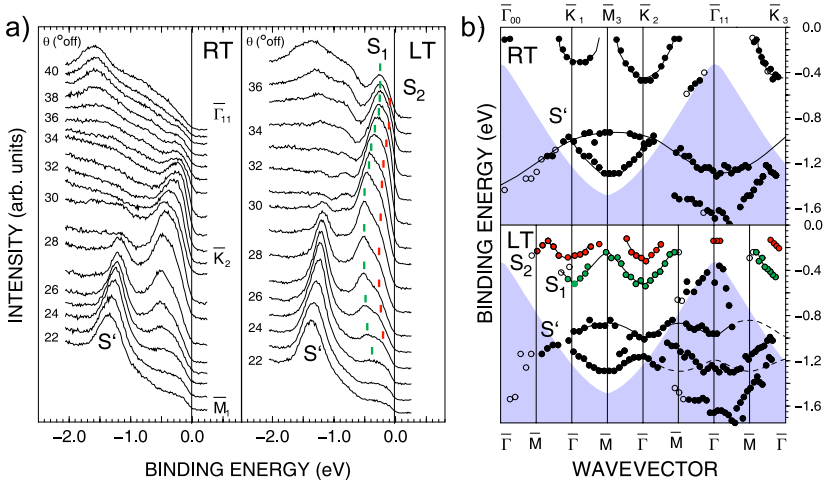

Figure 3. (a) Photoemission spectra as a function of emission angle θ along the $\overline{\Gamma K}$ direction of the RT-$\sqrt{3}$ phase, for the RT-$\sqrt{3}$ phase and the (3×3) phase (at 100 K). S′ is due to Pb p_x and p_y states, while S_1 and S_2 are related to Pb p_z states. (b) Energy versus momentum dispersion obtained from the experimental data of panel (a). Shadowed regions represent the projection of bulk states. The spectra are similar in both phases, with the exception of two changes: the electronic structure seen at RT is folded in the new LT symmetry and S_2 is more clearly split in two peaks at LT [25].

the (3×3) phase. One of them crosses the Fermi energy, making the (3×3) phase metallic. So, there is no significant difference between the electronic structure of both phases, suggesting that their atomic structures should be similar as well, and that the RT-$\sqrt{3}$ phase and the (3×3) phase are formed by the same building blocks. This indicates that the phase transition is induced by thermal disorder and should be of order–disorder type [13].

The possible role of nesting effects in the surface phase transition, as claimed in early studies [8], motivated an analysis of the Fermi surface of the RT-$\sqrt{3}$ phase of Pb/Ge(111) [25]. The experimental Fermi surface is shown in figure 4. At the moment when these data were measured, the true nature of the RT-$\sqrt{3}$ phase had not yet been established, and thus the experimental Fermi surface measured at RT was compared with the theoretical Fermi contour of an atomically flat $\sqrt{3}$ surface (figure 2(c)) [8, 9], whose Fermi surface is an undulated single sheet of $\sqrt{3}$ symmetry. The main question to answer at that moment was to what extent the undulation of the Fermi surface would indeed be compatible with a nesting mechanism, which requires flat areas in the Fermi surface. A comparison with well-known CDW compounds, such as $NaMo_6O_{17}$ or KMo_6O_{17}, reveals that a large percentage of flat areas has always been required to stabilize a CDW [52–56]. In the case of Pb/Ge(111), it was concluded that both the theoretical and the experimental Fermi surfaces are undulated, but the fraction of flat areas is insufficient to obtain a significant energy gain associated with a CDW instability [25]. In view of the fluctuating nature of the RT-$\sqrt{3}$ phase, its Fermi surface should rather be interpreted in terms of the electronic structure of the (3×3) phase. This anaysis is made later in this paper. The Fermi momentum was determined both from an analysis of the experimental band structure along the symmetry directions and directly from the Fermi surface. The Fermi vector k_F that is found is significantly larger along $\overline{\Gamma M}_{\sqrt{3}}$ (0.40 Å^{-1}) than along $\overline{\Gamma K}_{\sqrt{3}}$ (0.31 Å^{-1}). This measurement of k_F shows that the nesting condition for a (3×3) phase is fulfilled at most at a single point, along the $\overline{\Gamma K}$ direction of the RT-$\sqrt{3}$ phase.

An intriguing aspect of the phase transition in Pb/Ge(111) is the observation upon cooling of a pseudogap of ∼40 meV, which opens at the Fermi energy crossing along the $\overline{\Gamma M}$ direction

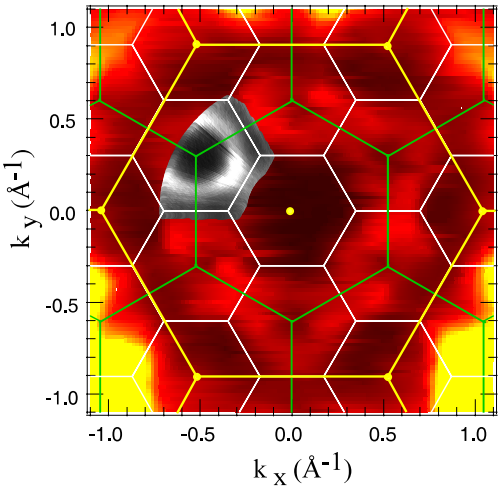

Figure 4. Experimental Fermi surface for the RT-$\sqrt{3}$ phase of Pb/Ge(111) measured with a conventional electron analyser (from [24]). The photoemission intensity is represented in a *yellow–red–black* colour scale (grey scale) for maxima and minima, respectively. Lines correspond to the (1 × 1) (yellow, large hexagons), ($\sqrt{3}$) (green, intermediate hexagons) and (3 × 3) (white, small hexagons) surface Brillouin zones. The small inset in grey scale is shown for comparison. It is extracted from the Fermi surface contours of figure 7 and it is measured with an image-type electron analyser. Except for the overall resolution improvement (energy and momentum), the agreement of both Fermi surfaces is remarkable.

of the (3 × 3) phase, and is observed as a decrease in the photoemission intensity and a small energy shift of the valence band onset [57, 58]. The pseudogap is unexpected in terms of electron counting, since the (3 × 3) phase is metallic. We speculate that it might be related to the phase transition at 76 K [41], but further work with higher resolution is needed to clarify this point. We note that a dip in the electron energy loss spectroscopy (EELS) quasi-elastic tail was observed in Pb/Ge(111)-(3 × 3) and that it was interpreted as a gap opening due to correlation effects [8]. Later work proposed a different interpretation, namely that that the dip could be due to image resonances [59].

2.2. Sn/Ge(111)

Soon after the discovery of the phase transition from the RT-$\sqrt{3}$ to the (3 × 3) structure on Pb/Ge(111), a similar transition was reported for Sn/Ge(111) [9], in this case at a slightly lower temperature. The Sn/Ge(111) interface presents a lower density of defects, consisting mostly of substitutional Ge atoms among the Sn adatoms. Thus, the Sn/Ge(111) interface is of higher quality than Pb/Ge(111) [9, 60, 61]. No gap opening was reported for Sn/Ge(111), and both the RT-$\sqrt{3}$ and the (3 × 3) phases are metallic. However, since STM images of empty and filled states at the (3 × 3) phase are complementary, it was initially argued that the atomic positions were not significantly modified along the phase transition, so that there was a charge rearrangement only, i.e. a weakly coupled CDW [9]. Density-functional theoretical calculations for Sn/Ge(111) indicated that nesting plays no role in the phase transition, because the most favourable point for nesting, which is along $\overline{\Gamma M}$ of the (3 × 3) phase, is 11% off commensurate, and the calculated Fermi vector is larger than the $\overline{\Gamma K}$ distance (figure 2(c)). Thus, the claimed CDW arrangement could not be explained by the Peierls mechanism [9], and correlation effects [9] and later the role of defects [10–12, 51] were invoked.

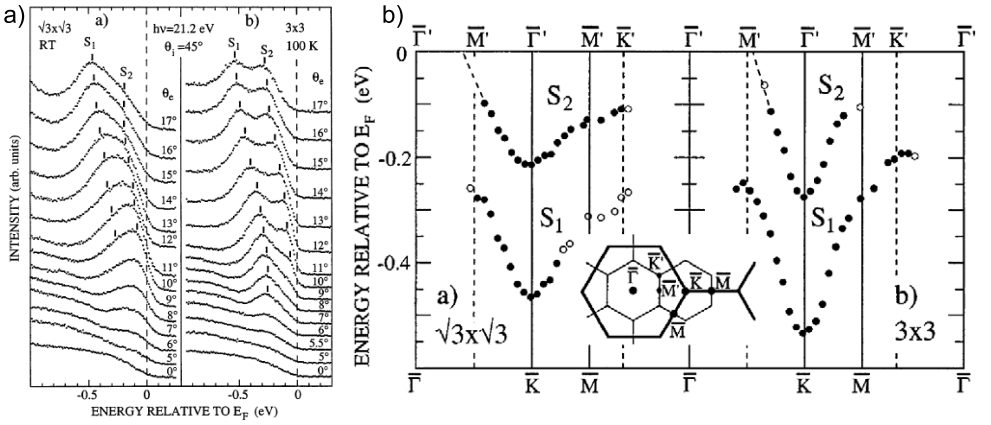

Figure 5. (a) Angle-resolved photoemission spectra along the $\overline{\Gamma K}$ direction of the RT-$\sqrt{3}$ surface Brillouin zone, measured for both the RT-$\sqrt{3}$ and the (3×3) phases. Two dispersive surface states are observed. (b) Band structure along the high-symmetry directions of the surface Brillouin zone. The symmetry points of the RT-$\sqrt{3}$ (3×3) phase are indicated at the bottom (top) of the panel. The inset shows the surface Brillouin zone. Both figures are extracted from [29].

Angle-resolved photoemission shows that Sn/Ge(111) and Pb/Ge(111) have a very similar electronic structure [13, 25, 29]. As in the case of Pb/Ge(111), the surface bands of both the RT-$\sqrt{3}$ phase and the (3×3) phase of Sn/Ge(111) (measured at 100 K) are identical, with two dispersive surface bands close to the Fermi energy. One of the two bands crosses the Fermi energy, as shown in figure 5 [29]. No evidence of significant electron correlation effects could be deduced from the surface electronic bands.

The strong similarity between the electronic structure of the RT-$\sqrt{3}$ and (3×3) phases means that the structure of the two phases should be the same. If this is the case, then not only the electronic structure near the Fermi level but also the Sn 4d core level line shape should reflect the similarity. The Sn 4d core level contains two main components, and shows almost the same line shape for both phases [13, 29, 62, 63]. As each component is related to a different chemical environment at the surface, the existence of two components in the Sn 4d core level reflects the presence of two kinds of Sn atoms at the surface [13, 29, 63]. In view of this evidence, the RT-$\sqrt{3}$ phase cannot be explained with a simple occupation of T_4 sites by equivalent Sn atoms, and so an atomically flat and metallic $\sqrt{3}$ surface does not exist, as supported by much other evidence [31–34]. A detailed understanding of the true nature of the RT-$\sqrt{3}$ phase is obtained from both first-principles molecular-dynamics simulations [13, 36] and from an analysis of the phonon dynamics of the surface as a function of temperature [36, 37]. Sn adatoms occupy well-defined vertical positions in the (3×3) structure. As the temperature increases, 'up' Sn adatoms are able to interchange vertical positions with 'down' Sn adatoms, in such a way that a local (3×3) structure is maintained. At intermediate temperatures, this flipping motion is moderate, but at RT it becomes important enough to destroy the (3×3) long-range order. This description, which is referred to as the 'dynamical fluctuations model', reminds us of dimer flipping in Si(100) [64]. Dimer flipping and ordering is behind the phase transition from a room-temperature (2×1) phase to a low-temperature $c(4 \times 2)$ phase in Si(100) [65–68]. Within the dynamical fluctuations model, STM observations are easily explained. STM is a slow probe, and at RT observes the average of the atomic positions of the vibrating atoms. In contrast, femtosecond (fs) sensitive techniques such as photoemission probe a 'frozen' (3×3) structure, even at RT, since both phases are structurally

identical at the local level on the femtosecond timescale [13, 34, 36, 37]. The up and down movement of Sn adatoms has recently been observed by analysing the time dependence of the tunnelling current above the Sn atoms [34], which is direct confirmation of the model. Also, results from x-ray standing waves (XSW) using fluorescence as an inelastic probe support that the RT-$\sqrt{3}$ phase contains one-third of the Sn atoms higher than the remaining two-thirds [33]. The phase transition is driven by freezing of the oscillations of Sn adatoms, as observed experimentally [36, 37]. It is important to point out that this 'up–down' freezing should not be confused with the soft phonon required by the Peierls mechanism. The phase transition is therefore of order–disorder type, in agreement with several other experiments, such as He scattering [31] or photoelectron diffraction [32].

All the above evidence supports a structural model for the (3×3) reconstruction consisting of one upward ('up') and two downward ('down') displaced Sn atoms per unit cell. This configuration is commonly called the '1U2D model', and it corresponds to a direct interpretation of the bright spots in the STM images as being due to atoms protruding from the surface, in agreement with theoretical calculations on the origin of the STM images [26]. This picture is further supported by surface x-ray diffraction (SXRD) experiments, performed first for Pb/Ge(111) [35] and later for Sn/Ge(111) [69, 70] and by dynamical low-energy electron diffraction (LEED) [70]. SXRD has shown that the substrate participates significantly in this 'up–down' distortion, which strongly affects the three Ge atoms directly bonded to each adatom (Sn, Pb), and several Ge layers underneath [35]. Photoelectron diffraction experiments show unambiguously that the RT and LT phases have the same structure and present two kinds of atoms [32, 71, 72]. Finally, XSW, using fluorescence as an inelastic probe [33, 73], has also supported the 1U2D model. From the theoretical point of view, several *ab initio* calculations have found that the ground state of Sn/Ge(111) is a buckled (3×3) structure [13, 74, 75]. So, the 1U2D model for the (3×3) phase is supported by a compelling combination of experimental and theoretical evidence.

In spite of the general agreement reached on most of the properties of both the RT-$\sqrt{3}$ and the (3×3) phases described above, the Sn 4d core-level line-shape is not yet well understood. As mentioned above, the Sn 4d core level contains two different components in an approximate ratio of 1:2, in agreement with the 1U2D model. The existence of two different kinds of atoms in the unit cell also explains why the surface band closest to the Fermi energy is split into two different surface states: one fully occupied, and the other one crossing the Fermi energy. Indeed, due to the height difference, there is charge transfer from the two 'down' atoms towards the 'up' atom, so that one of the surface bands (localized mainly on the 'up' atom) becomes filled, and each 'down' surface atom contributes with only $1/4$ electron to the half-filled band, which crosses the Fermi energy. Due to the charge transfer, the Sn 4d core-level component associated with the 'up' atoms should appear at lower BE than the component associated with 'down' atoms, within an initial-state interpretation. The largest component (which should correspond to the two 'down' atoms) appears at higher BE than the smallest component. This is opposite to the prediction of an initial state model, as summarized above. Different explanations have been put forward to explain this reversal, such as photoemission final-state effects [13], which are known to affect the BE position of surface core-level components in semiconducting interfaces [76]. However, doping experiments [17, 61, 77] conclude that the low-BE component of the Sn 4d core level has a filled valence state character, i.e. the assignment expected from an initial state model. Following this argument, and in view of the relative intensities of the two Sn 4d components, the (3×3) phase should be described as a 2U1D structure. X-ray standing wave experiments for the RT-$\sqrt{3}$ phase using the Sn 3d core level as an inelastic signal [78] have also found that the low-BE component corresponds to the 'up' atom. The interpretation of these studies contradicts the conclusions accumulated from

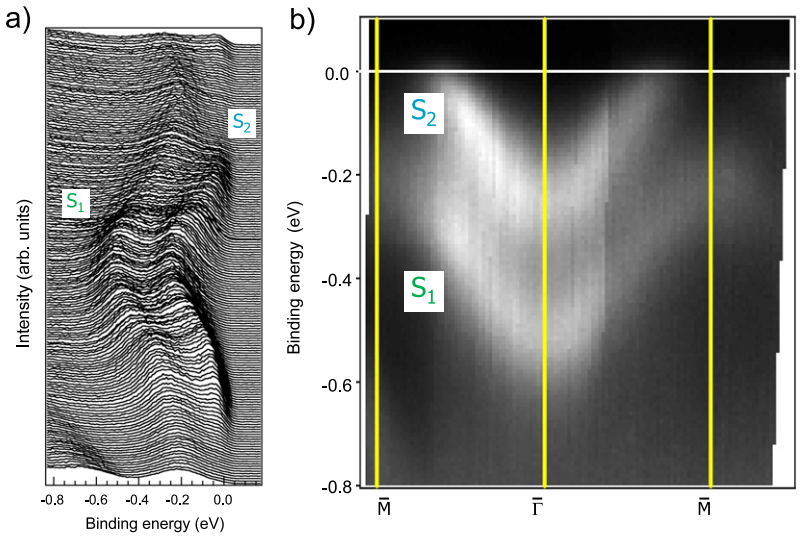

Figure 6. Experimental band structure for the (3 × 3) phase along the $\overline{\Gamma M}$ symmetry direction taken with a two-dimensional electron detector. (a) Angle-resolved spectra. (b) Two-dimensional representation of the data from panel (a). Notice the existence of the two well-resolved and dispersive surface states S_1 and S_2. S_2 crosses the Fermi level, leading to a metallic phase. S_1 is backfolded at $\overline{M}$ points [22].

a large variety of experimental probes. Possibly, the only way out to solve this long-standing controversy is to perform higher-resolution measurements on the core-level line-shape.

Following the discussion above, it is clear that the surface electronic structure is closely related to the 'up–down' buckling in the surface unit cell. Figure 6 shows angle-resolved photoemission spectra along the $\overline{\Gamma M}$ direction for Sn/Ge(111)-(3 × 3). The data are taken with an image-type electron analyser with state-of-the-art resolution. Two surface bands are observed. The first one is completely filled (S_1) and the second one (S_2) crosses the Fermi energy and makes the surface metallic. The data are in good agreement with theoretical calculations in the local-density approximation (LDA) for a buckled ground state [30, 79, 80]. In these calculations, the S_1/S_2 splitting is unambiguously related to the presence of inequivalent Sn atoms in the (3 × 3) unit cell. The splitting is due to the charge transfer between 'up' and 'down' atoms in an ideal surface, and defects do not play any role in it. S_1 is mainly weighted on the 'up' Sn atoms, while the metallic band S_2 is associated with the 'down' Sn atoms [13, 81]. The absolute band splitting is related to the corrugation in the Sn layer, because the structural height difference reflects the charge transfer from the lower to the higher dangling bond. The details of this process have been described in several theoretical works [30]. As summarized above, since Sn atoms have a threefold bonding, there is one electron per dangling bond, and three surface bands per (3 × 3) unit cell. These bands are calculated to be narrow (∼0.2 eV) and, due to the intra-site Coulomb interaction of ∼0.55 eV, correlation effects could be significant [27, 28, 82], although the (3 × 3) phase is still metallic and non-magnetic [74]. The Sn atom associated with the lower band completely fills its dangling bond, so the Ge–Ge bond along the (111) direction is strengthened while the Sn–Ge bond is weakened, and so the adatom rises. In contrast, the other two Sn atoms move downwards due to the partial depopulation of their orbitals. Therefore, the lowest band

has more sp^3-like character due to rehybridization and is related to the Sn atoms displaced upwards, while the other metallic bands with one electron per unit cell are associated with the atoms displaced downwards [28, 81, 83].

We conclude from these arguments that the charge transfer depends on the structure of the surface, and we can expect that transferring charge from two Sn atoms in the down position to one atom in the up position (the 1U2D model) should be different from having only one atom in the down position, which provides charge to two Sn atoms in up positions (the 2U1D model). The electronic band structure of the two rippled structures, 1U2D and 2U1D, and of a flat $\sqrt{3}$ phase, has been calculated within the density-functional approach [80, 84, 85]. These calculations conclude first that the surface band splitting is related to the rippling, and second that major changes are expected at the $\overline{\mathrm{K}}$ point of the (3×3) phase, depending on whether the rippling is 1U2D or 2U1D. While for the 1U2D structure there is a surface band with a BE of approximately 0.3–0.5 eV at $\overline{\mathrm{K}}$, the band moves above the Fermi energy in the 2U1D configuration. The experimental data show one single band with 0.4 eV BE and no intensity at the Fermi level along the $\overline{\mathrm{MK}}$ direction (figure 5(a)), supporting the 1U2D model.

3. The Fermi surface

The Fermi surface of bulk materials is studied using several different techniques, such as the magneto-acoustic effect [86], the anomalous skin effect [87], positron annihilation [88–90] and mainly the de Haas–van Alphen effect [91]. More recently, Compton scattering has also been used to probe the Fermi surface topology [92–94]. While all these techniques offer powerful ways to probe the Fermi surface of crystalline solids, angle-resolved photoemission becomes the technique of choice whenever no large single-crystalline samples are available, if the Brillouin zone is small or if the surface is significatively modified. In the case of low-dimensional materials, only angle-resolved photoemission can probe the Fermi surface. The main feature of this technique is its capacity to measure the density of occupied states with momentum resolution (spectral function). This capability can be exploited to determine the Fermi surface by selecting a narrow energetic window around the Fermi level, and by measuring the photoemission intensity in this window for a whole reciprocal-space hemisphere [95, 96]. Depending on the selected BE, constant-energy surfaces can also be measured besides the Fermi surface. In the case of three-dimensional crystals, a photoemission experiment at constant photon energy measures a two-dimensional cut of the three-dimensional Fermi surface. Further cuts with different photon energies are required to map the whole three-dimensional Fermi surface. In a true two-dimensional material, the whole (two-dimensional) Fermi contour is obtained directly with a single photon energy. We refer the reader to [95, 96] and to other contributions in this special section for a more detailed account on this method.

The information provided by the Fermi surface is particularly interesting in materials close to instabilities, because their properties are critically determined by the electronic states closest to the Fermi energy. As an example, we may mention surface CDWs [96–108], bulk CDWs [109], systems with enhanced electron–phonon coupling [110], cuprate superconductors [111], manganites [112], graphene [113], etc.

In spite of the importance of an accurate knowledge of the Fermi surface of the Sn, Pb/Ge(111) interfaces, only the Fermi surface of the RT-$\sqrt{3}$ phase has been measured with moderate energy and angle resolution, as described above, both for Pb/Ge(111) [25, 114] and Sn/Ge(111) [115]. From a simple inspection of the (3×3) theoretical band structure (see figure 1(d)), we expect a single-sheet Fermi surface, formed by an electron-like contour centred at the $\overline{\Gamma}$ points. Figure 7 shows a series of selected experimental contours, including the Fermi surface and several other constant-energy surfaces, measured for increasingly higher

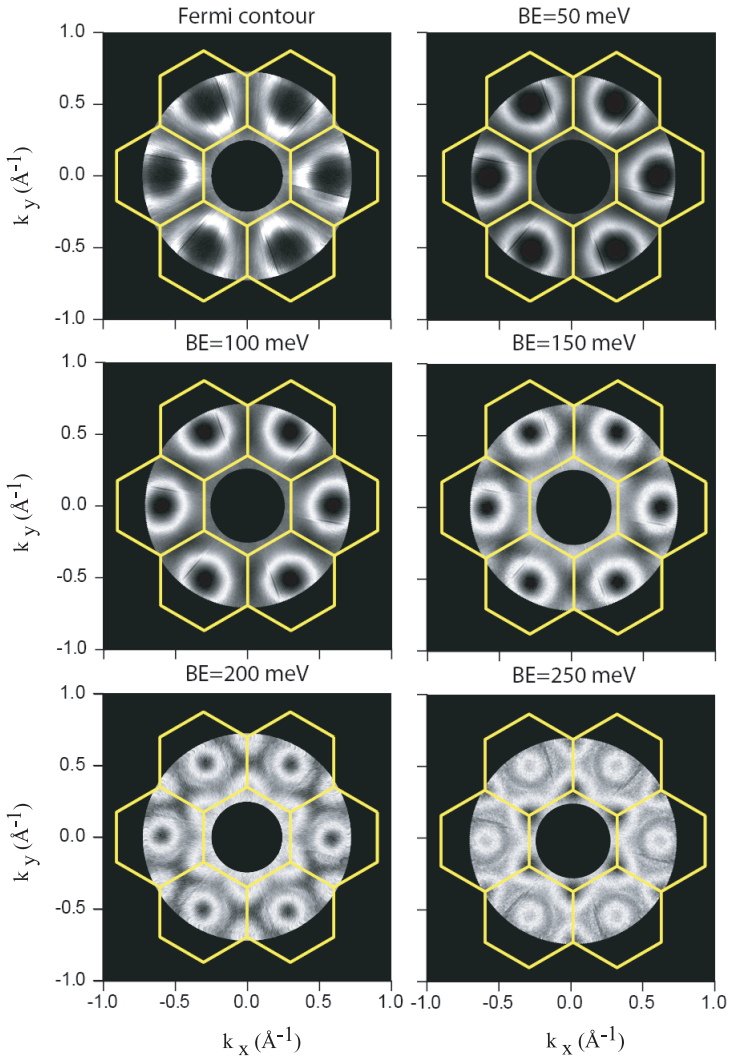

Figure 7. Experimental constant-energy surfaces ($h\nu = 21$ eV) for an energy-integrated window of ±5 meV around binding energies of 0 meV (Fermi surface), 50, 100, 150, 200 and 250 meV. Bright colour means higher intensity. The surface Brillouin zone of the (3 × 3) Sn/Ge(111) is superimposed. The temperature was kept at 100 K. Data have been acquired over a 60° azimuthal sector and symmetrized.

BEs. All the contours were measured at 100 K. The overall energy resolution is 9 meV, while the angular resolution is 0.1° along the radial direction and 1.1° at least along the azimuthal direction. The data were measured with a state-of-the-art two-dimensional electron detector. The Fermi surface and the other constant-energy surfaces were acquired simultaneously.

Relevant information can be gained from an analysis of the Fermi surface shape. The Fermi surface is an almost circular contour centred at the $\overline{\Gamma}$ point. The Fermi vector k_F along $\overline{\Gamma M}$ (0.203 $Å^{-1}$) is slightly smaller (∼10%) than along $\overline{\Gamma K}$ (0.214 $Å^{-1}$), so the Fermi surface is not exactly circular. These values compare well with theoretical calculations [30, 80]

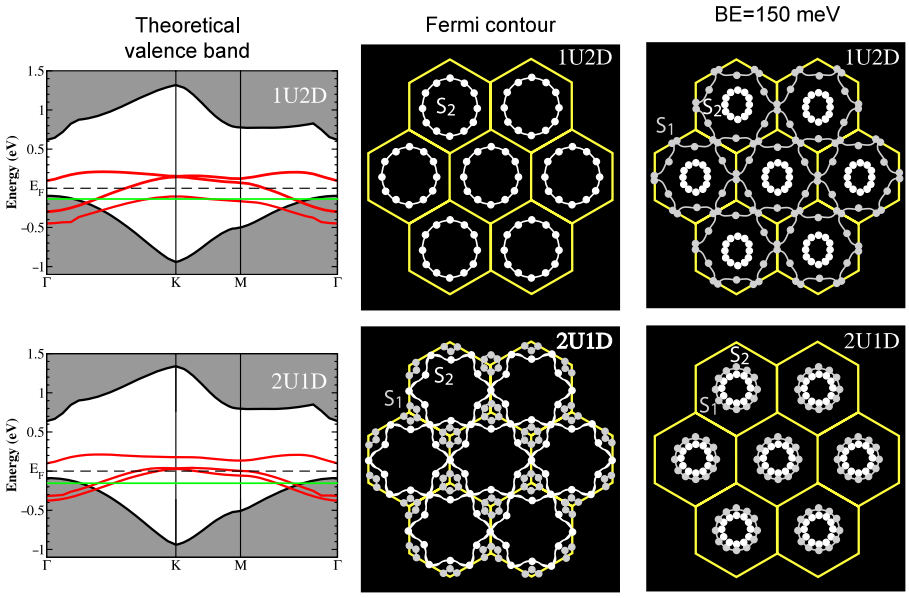

Figure 8. Left: LDA theoretical band structure calculated for the 1U2D and the 2U1D structures, from [74]. The horizontal green (grey) line corresponds to a 150 meV BE. Centre: schematic representation of the theoretical Fermi surface from the band structure of the left-hand column for the 1U2D and the 2U1D structures. Right: same as the central column, but for constant-energy surfaces corresponding to a BE of 150 meV. The white (grey) points in the Fermi contours and constant-energy surfaces correspond to surface state S_2 (S_1).

($\overline{\Gamma M} = 0.184$ Å^{-1} and $\overline{\Gamma K} = 0.204$ Å^{-1}), although experimental values are smaller and the Fermi contour is more rounded than theoretical predictions. The Fermi surface does not contact the hexagon of the (3×3) Brillouin zone edge (0.302 Å^{-1} for $\overline{\Gamma M}$ and 0.349 Å^{-1} for $\overline{\Gamma K}$), and indeed it is so far away from it that nesting from a hypothetical flat $\sqrt{3}$ phase is also discarded. There are no indications of any Peierls gaps at $\overline{M}$, so CDW models (or even the suggested sliding CDW models [51]), either based on the Peierls mechanism or on gapping, are discarded by these high-resolution experimental measurements. The absolute filling of a band crossing the Fermi energy can also be determined from the area of the Fermi contour, assuming the validity of the two-dimensional Luttinger count [116]. A numerical integration of the Fermi contour area results in a filling of (0.92 ± 0.05) electrons, which is close to the expected value of 1.0 electrons.

An analysis of the Fermi surface and of the different constant-energy surfaces can discriminate whether the atomic structure of the surface is 1U2D, 2U1D or flat. An advantage of this method it that photoemission experiments average over large sample areas and the signal is dominated by the most stable structure. This is not the case for scanning microscopies like STM, which provide information on a local scale. A visual inspection of the experimental data shown in figure 7 reveals that, as the BE increases, the radius of the Fermi contour decreases, as expected for an electron-like band. No other feature is experimentally detected down to 150 meV BE. At this point, some intensity appears around the $\overline{K}$ points. For an even slightly larger BE, circular contours centred at $\overline{K}$ appear whose radius increases with BE, as expected for a hole-like band. In order to interpret this data, we come back to the theoretical calculations of Pulci *et al* [80, 85], who have compared the electronic band structures of the 1U2D and 2U1D models. In figure 8 we show the shape of selected contours, together with a schematic

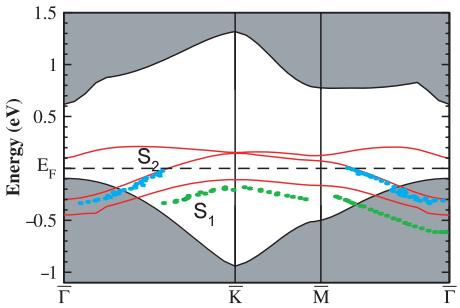

Figure 9. Comparison between the theoretical and experimental bands for the (3×3) phase. Lines correspond to calculations for the 1U2D model [80]. Circles correspond to experimental points obtained either from constant-energy surfaces or from standard dispersions.

representation of the theoretical Fermi surface and the corresponding constant-energy surface for 150 meV BE. This BE is marked as a green line in the theoretical valence band structure on the left. The contours for the 1U2D and 2U1D models are compared in this figure by representing in reciprocal space the constant-energy intersections of the theoretical electron bands for each structure. From this plot and from the band structure itself, it is clear that only the 1U2D structure has no features around $\overline{\mathrm{K}}$ at the Fermi level, as observed in the experimental constant-energy surfaces.

On the other hand, the intensity around $\overline{\mathrm{K}}$ is detected for BEs above 150 meV. Figure 7 shows a hole-like band around $\overline{\mathrm{K}}$ points for binding energies of 200 and 250 meV. In agreement with theoretical calculations for the 1U2D structure [75, 80], this contour around $\overline{\mathrm{K}}$ is not exactly circular. For a 250 meV BE, the cut along the $\overline{\mathrm{KM}}$ direction (0.132 $\mathrm{\AA}^{-1}$) is larger than along the $\overline{\mathrm{K\Gamma}}$ direction (0.085 $\mathrm{\AA}^{-1}$). The constant-energy surfaces for 200 and 250 meV also show two concentric quasi-circular contours centred at $\overline{\Gamma}$. The inner circle corresponds to the band crossing the Fermi energy, as its radius decreases with increasing BE. The outer circle, which is observed only for a narrow range of BEs, shows several specific properties, such as a narrower width in reciprocal space, specific symmetry, and overall weak intensity. This outer circle is due to a bulk band, previously reported for the same reciprocal space location [117]. The bulk band is traced back to a (3×3) Umklapp of a Ge bulk band from the conduction band maximum, which appears at normal emission.

All these arguments are made more explicit by plotting an experimental energy versus momentum dispersion relationship, which can be obtained from the constant-energy surfaces. This is made by measuring the BE versus momentum along high-symmetry directions (figure 6). Points with BEs smaller than 250 meV in figure 7 are obtained in this way. Additional data with a higher BE are also included for completeness. Figure 9 compares the experimental band structure with the theoretical predictions for the 1U2D model. The agreement between theory and experiment (dispersion and BE) is remarkable for the metallic surface band that generates the Fermi surface (S_2). The dispersion of the second (completely filled) surface band (S_1) is also well described, although the experimental data points are shifted by 75 meV to higher BE. This discrepancy could be attributed to the difficulty for LDA calculations to take into account the exchange and correlation energy. In this case, we would expect a uniform shift of LDA bands towards larger BEs, as observed for S_1. However, such effects can be discarded in the case of Sn/Ge(111), in view of the excellent agreement found for S_2. It is indeed the splitting between the two bands that is slightly underestimated by the calculation. Since the splitting between the two surface bands is

induced by the up–down distortion in the Sn layer, we conclude that the larger experimental splitting reflects a distortion that is higher than calculated (0.37 Å) [80]. In summary, a comparison between the experimental band structure and theoretical calculations shows that, except for minor discrepancies, the experimental data are in very good agreement with LDA calculations [13, 80, 85] predicting a 1U2D configuration.

It is also very clarifying to devote some time to previous studies of the Fermi surface of Sn/Ge(111) and Pb/Ge(111) and their agreement with the results reported here. A direct measurement of the whole Fermi surface has only been accomplished before for the RT-$\sqrt{3}$ phase of both Sn/Ge(111) [115] and Pb/Ge(111) [25, 114]. The experimental Fermi surfaces of both interfaces are almost identical. The RT-$\sqrt{3}$ phase is a mixture of local (3×3) configurations, fluctuating on a picosecond timescale [13, 36]. When probed on the femtosecond timescale typical of photoemission, it should exhibit the features of the (3×3) phase. This argument is exact in the case of the Sn 4d core level. In the valence band of the RT-$\sqrt{3}$ phase, we expect to observe a band splitting, because there is a local (3×3) structure and charge transfer between up and down Sn atoms. However, we do not expect to observe features related to the (3×3) long-range order, such as band folding. In summary, the Fermi surface of the RT-$\sqrt{3}$ phase should be similar to the Fermi surface of the (3×3) phase when probed at the femtosecond timescale of photoemission, although broadened due to thermal effects, but with weaker (or missing) (3×3) band folding. A direct comparison with the data measured ten years ago with a lower resolution reveals that this is indeed the case. At RT the sharp contour shown in figure 7 is detected as a diffuse spot centred anyway at $\overline{\Gamma}$ (see figure 4). Due to the lack of (3×3) long-range order at RT, a larger intensity is detected around the $\sqrt{3}$ zone edge, because the surface band is located around the $\overline{\mathrm{K}}_{\sqrt{3}}$ points. Due to the lack of (3×3) band folding, there is almost no intensity at the $\overline{\Gamma}$ points of the (3×3) phase which are not $\overline{\mathrm{K}}_{\sqrt{3}}$ points. Taking into account this effect, and that photoemission matrix elements also generate different apparent intensities in different Brillouin zones, the RT-$\sqrt{3}$ data are in excellent agreement with the predictions of the dynamical fluctuations model and the Fermi surface of the (3×3) phase reported in this work.

Chiang *et al* [51, 118] have compared the electronic band structures of the RT-$\sqrt{3}$ phase and the (3×3) phase. They proposed that the RT surface bands could contain a contribution from a flat, metallic $\sqrt{3}$ phase and of (3×3) domains nucleated around defects. However, their valence band line-shape near the $\overline{\Gamma}$ point ($\overline{\mathrm{K}}$ in the notation of the $\sqrt{3}$ Brillouin zone) is in disagreement with the results of other groups. First, the two surface states are hardly resolved. Second, their relative intensity is reversed with respect to what is known to correspond to a well-ordered surface for the correct Sn coverage. Due to this fact, either excessively low energetic or angular resolution was used, or the surface that was analysed did not correspond to the correct Sn coverage, which makes the proposed model doubtful.

4. Conclusions

In this article we review the electronic band structure and Fermi surface data for Sn/Ge(111) and Pb/Ge(111), with an emphasis on new results obtained at 110 K with state-of-the-art resolution. The electronic surface bands that are found are in very good agreement with the predictions of density functional calculations. The (3×3) phase is metallic, with an electron-like Fermi contour centred at the $\overline{\Gamma}$ points. The Fermi contour is smaller than the (3×3) Brillouin zone and there are no signs of gapping. The surface electronic band structure is extremely sensitive to the vertical arrangement of the two inequivalent Sn atoms in the surface unit cell. In consequence, the shape of the Fermi surface and of constant-energy surfaces becomes highly

dependent on the surface morphology. We report a detailed analysis of the Fermi surface and constant-energy surface topology which allows us to discern the atomic structure of the system. We conclude that the (3×3) reconstruction consists of a unit cell with one Sn atom displaced upwards and two displaced downwards (1U2D model). The atoms oscillate vertically at RT, which produces the RT-$\sqrt{3}$ phase, but at lower temperatures the oscillations are frozen and a (3×3) reconstruction is observed, in agreement with the predictions of the dynamical fluctuations model. More experimental data with higher resolution are needed to solve the long-term controversy concerning the interpretation of the Sn 4d core-level line-shape.

Acknowledgments

We acknowledge financial support from Ministerio de Educación y Ciencia (Spain) under grant nos FIS2006-04552 and FIS2005-0747 and from Comunidad de Madrid (Programme S-0505/PPQ/0316). RC thanks Comunidad de Madrid and Fondo Social Europeo. Part of this work was performed at the Swiss Light Source, Paul Scherrer Institut, Villigen, Switzerland.

References

[1] Persson B N J 1992 *Surf. Sci. Rep.* **15** 1
[2] Sambandamurthy G, Engel L W, Johansson A, Peled E and Shahar D 2005 *Phys. Rev. Lett.* **94** 017003
[3] Imada M, Fujimori A and Tokura Y 2001 *Rev. Mod. Phys.* **70** 1039
[4] Aruga T 2006 *Surf. Sci. Rep.* **61** 283
[5] Aruga T 2002 *J. Phys.: Condens. Matter* **14** 8393
[6] Tosatti E 1995 *Electronic Surface and Interface States on Metallic Systems* ed E Bertel and M Donath (Singapore: World Scientific)
[7] Bune A V, Fridkin V M, Ducharme S, Blinov L M, Palto S P, Sorokin A V, Yudin S G and Zlatkin A 1998 *Nature* **391** 874
[8] Carpinelli J M, Weitering H H, Plummer E W and Stumpf R 1996 *Nature* **381** 398
[9] Carpinelli J M, Weitering H H, Bartkowiak M, Stumpf R and Plummer E W 1997 *Phys. Rev. Lett.* **79** 2859
[10] Melechko A V, Braun J, Weitering H H and Plummer E W 1999 *Phys. Rev. Lett.* **83** 999
[11] Weitering H H, Carpinelli J M, Melechko A V, Zhang J, Bartkowiak M and Plummer E W 1999 *Science* **285** 2107
[12] Melechko A V, Braun J, Weitering H H and Plummer E W 2000 *Phys. Rev.* B **61** 2235
[13] Avila J, Mascaraque A, Michel E G, Asensio M C, LeLay G, Ortega J, Pérez R and Flores F 1999 *Phys. Rev. Lett.* **82** 442
[14] Morikawa H, Matsuda I and Hasegawa S 2002 *Phys. Rev.* B **65** R201308
[15] Pérez R, Ortega J and Flores F 2001 *Phys. Rev. Lett.* **86** 4891
[16] Custance O, Brihuega I, Veuillen J Y, Gómez-Rodríguez J M and Baró A M 2001 *Surf. Sci.* **482–485** 1399
[17] Dudr V, Tsud N, Fabík S, Vondráek M, Matolín V, Cháb V and Prince K C 2004 *Phys. Rev.* B **70** 155334
[18] Brihuega I, Custance O, Pérez R and Gómez-Rodríguez J M 2005 *Phys. Rev. Lett.* **94** 046102
[19] Ichikawa T and Ino S 1981 *Surf. Sci.* **105** 395
[20] Ichikawa T 1983 *Solid State Commun.* **48** 827
[21] Metois J J and LeLay G 1983 *Surf. Sci.* **133** 422
[22] Cortés R, Tejeda A, Lobo J, Didiot C, Kierren B, Malterre D, Michel E G and Mascaraque A 2006 *Phys. Rev. Lett.* **96** 126103
[23] Nagayoshi H 1994 *Surf. Rev. Lett.* **1** 369
[24] Nogami J 1994 *Surf. Rev. Lett.* **1** 395
[25] Mascaraque A, Avila J, Michel E G and Asensio M C 1998 *Phys. Rev.* B **57** 14758
[26] Jurczyszyn L, Ortega J, Pérez R and Flores F 2001 *Surf. Sci.* **482–485** 1350
[27] Santoro G, Scandolo S and Tossati E 1999 *Phys. Rev.* B **59** 1891
[28] Flores F, Ortega J, Pérez R, Charrier A, Thibaudau F, Deveber J-M and Themlin J-M 2001 *Prog. Surf. Sci.* **67** 299
[29] Uhrberg R I G and Balasubramanian T 1998 *Phys. Rev. Lett.* **81** 2108
[30] Ortega J, Pérez R and Flores F 2002 *J. Phys.: Condens. Matter* **14** 5979

[31] Floreano L, Cvetko D, Bavdek G, Benes M and Morgante A 2001 *Phys. Rev.* B **64** 075405
[32] Petaccia L, Floreano L, Goldoni A, Cvetko D, Morgante A, Grill L, Verdini A, Commelli G, Paolucci G and Modesti S 2001 *Phys. Rev.* B **64** 193410
[33] Okasinski J S, Kim C-Y, Walko D A and Bedzyk M J 2004 *Phys. Rev.* B **69** 041401(R)
[34] Ronci F, Colonna S, Thorpe S D, Cricenti A and LeLay G 2005 *Phys. Rev. Lett.* **95** 156101
[35] Mascaraque A, Avila J, Alvarez J, Asensio M C, Ferrer S and Michel E G 1999 *Phys. Rev. Lett.* **82** 2524
[36] Farías D, Kamiski W, Lobo J, Ortega J, Hulpke E, Pérez R, Flores F and Michel E G 2003 *Phys. Rev. Lett.* **91** 16103
[37] Lobo J, Farías D, Hulpke E and Michel E G 2005 *Phys. Rev.* B **71** 205402
[38] Ortega J, Pérez R, Jurczyszyn L and Flores F 2002 *J. Phys.: Condens. Matter* **14** 7147
[39] Cano A, Levanyuk A P and Michel E G 2005 *Z. Kristallogr.* **220** 663
[40] Cano A, Levanyuk A P and Michel E G 2005 *Nanotechnology* **16** 325
[41] Guo J, Shi J and Plummer E W 2005 *Phys. Rev. Lett.* **94** 036105
[42] Erwin S C 2006 *Nature* **441** 295
[43] Brihuega I, Custance O, Ugeda M M, Oyabu N, Morita S and Gómez-Rodríguez J M 2005 *Phys. Rev. Lett.* **95** 206102
[44] Northrup J E 1984 *Phys. Rev. Lett.* **53** 683
[45] Carlisle J A, Miller T and Chiang T-C 1993 *Phys. Rev.* B **47** 10342
[46] Kinoshita T, Kono S and Sagawa T 1986 *Phys. Rev.* B **34** 3011
[47] Nicholls J M, Martensson P, Hansson G V and Northrup J E 1985 *Phys. Rev.* B **32** 1333
[48] Goldoni A, Cepek C and Modesti S 1997 *Phys. Rev.* B **55** 4109
[49] Seehofer L, Falkenberg G and Johnson R L 1993 *Surf. Sci.* **290** 15
[50] Karlsson C J, Landemark E, Chao Y C and Uhrberg R I G 1992 *Phys. Rev.* B **45** 6321
[51] Chiang T-C, Chou M Y, Kidd T and Miller T 2002 *J. Phys.: Condens. Matter* **14** R1
[52] Gweon G H, Allen J W, Clack J A, Zhang Y X, Poirier D M, Benning P J, Olson C G, Marcus J and Schlenker C 1997 *Phys. Rev.* B **55** R13353
[53] Grüner G 1994 *Density Waves in Solids* (Reading, MA: Addison-Wesley)
[54] Tosatti E 1975 *Festkoerperprobleme* **XV** 113
[55] Roca L, Mascaraque A, Avila J, Drouard S, Guyot H and Asensio M C 2004 *Phys. Rev.* B **69** 075114
[56] Mascaraque A, Roca L, Avila J, Drouard S, Guyot H and Asensio M C 2002 *Phys. Rev.* B **66** 115104
[57] Mascaraque A, Avila J, Michel E G and Asensio M C 1998 *Surf. Sci.* **402–404** 742
[58] Avila J, Mascaraque A, Michel E G and Asensio M C 1998 *Appl. Surf. Sci.* **123/124** 626
[59] Petaccia L, Grill L, Zangrando M and Modesti S 1999 *Phys. Rev. Lett.* **82** 386
[60] Göthelid M, Hammar M, Tönevik C, Karlsson U O, Nilsson N G and Flodström S A 1992 *Surf. Sci.* **271** L357
[61] Göthelid M, Grehk T M, Hammar M, Karlsson U O and Flodström S A 1995 *Surf. Sci.* **328** 80
[62] Göthelid M, Björkqvist M, Grehk T M, Le Lay G and Karlsson U O 1995 *Phys. Rev.* B **52** R14352
[63] Uhrberg R I G and Balasubramanian T 2000 *Phys. Rev. Lett.* **85** 1036
[64] Alerhand O L, Nihat Berker A, Joannopoulos J D, Vanderbilt D, Hamers R J and Demuth J E 1990 *Phys. Rev. Lett.* **64** 2406
[65] Tabata T, Aruga T and Murata Y 1987 *Surf. Sci.* **179** L63
[66] Landemark E, Karlsson C J, Chao Y-C and Uhrberg R I G 1992 *Phys. Rev. Lett.* **69** 1588
[67] Landemark E, Karlsson C J, Chao Y-C and Uhrberg R I G 1993 *Surf. Sci.* **287/288** 529
[68] Kubby J A and Boland J J 1996 *Surf. Sci. Rep.* **26** 61
[69] Bunk O, Zeysing J H, Falkenberg G, Johnson R L, Nielsen M, Nielsen M M and Feidenhans'l R 1999 *Phys. Rev. Lett.* **83** 2226
[70] Zhang J, Ismail, Rous P J, Baddorf A P and Plummer E W 1999 *Phys. Rev.* B **60** 2860
[71] Floreano L, Petaccia L, Benes M, Cvetko D, Goldoni A, Gotter R, Grill L, Morgante A, Verdini A and Modesti S 1999 *Surf. Rev. Lett.* **6** 1091
[72] Petaccia L, Floreano L, Benes M, Cvetko D, Goldoni A, Grill A, Morgante A, Verdini A and Modesti S 2001 *Phys. Rev.* B **63** 115406
[73] Escuadro A A, Goodner D M, Okasinski J S and Bedzyki M J 2004 *Phys. Rev.* B **70** 235416
[74] de Gironcoli S, Scandolo S, Ballabio G, Santoro G and Tosatti E 2000 *Surf. Sci.* **454–456** 172
[75] Gori P, Pulci O and Cricenti A 2006 *Japan. J. Appl. Phys.* **45** 2140
[76] Pehlke E and Scheffler M 1993 *Phys. Rev. Lett.* **71** 2338
[77] Dávila M E, Avila J, Asensio M C and LeLay G 2004 *Phys. Rev.* B **70** 241308
[78] Lee T-L, Warren S, Cowie B C C and Zegenhagen J 2006 *Phys. Rev. Lett.* **96** 046103
[79] Ballabio G, Profeta G, de Gironcoli S, Scandolo S, Santoro G E and Tosatti E 2002 *Phys. Rev. Lett.* **89** 126803
[80] Gori P, Pulci O and Cricenti A 2006 *J. Physique* IV **132** 91

[81] Ortega J, Pérez R and Flores F 2000 *J. Phys.: Condens. Matter* **12** L21
[82] Flores F, Ortega J and Pérez R 1999 *Surf. Rev. Lett.* **6** 411
[83] Ortega J, Flores F, Pérez R and Levy Yeyati A 1998 *Prog. Surf. Sci.* **59** 233
[84] Ortega J, Pérez R and Flores F, private communication
[85] Pulci O, Marsili M, Gori P, Palummo M, Cricenti A, Bechstedt F and del Sole R 2006 *Appl. Phys.* A **85** 361
[86] Cohen M H 1960 *Phys. Rev.* **117** 937
[87] Pippard A B 1957 *Phil. Trans. R. Soc.* A **250** 325
[88] Lock D G, Crisp V H C and West R N 1973 *J. Phys. F: Met. Phys.* **3** 561
[89] Biasini M, Ferro G, Kontrym-Sznajd G and Czopnik A 2002 *Phys. Rev.* B **66** 075126
[90] Laverock J, Dugdale S B, Major Zs, Alam M A, Ru N, Fisher I R, Santi G and Bruno E 2005 *Phys. Rev.* B **71** 085114
[91] de Haas W J and van Alphen P M 1930 *Leiden Comm.* 208d, 212a
[92] Cooper M J 1985 *Rep. Prog. Phys.* **48** 415
[93] Sakurai Y, Tanaka Y, Bansil A, Kaprzyk S, Stewart A T, Nagashima Y, Hyodo nT, Nanao S, Kawata H and Shiotani N 1995 *Phys. Rev. Lett.* **74** 2252
[94] Hiraoka N, Buslaps T, Honkimaki V, Ahmad J and Uwe H 2007 *Phys. Rev.* B **75** R121101
[95] Aebi P, Osterwalder J, Fasel R, Naumovic D and Schlapbach L 1994 *Surf. Sci.* **307–309** 917
[96] Kevan S D 1995 *J. Electron Spectrosc. Relat. Phenom.* **75** 175
[97] Tosatti E 1978 *Solid State Commun.* **25** 637
[98] Debe M K and King D A 1977 *J. Phys. C: Solid State Phys.* **10** L303
[99] Felter T E, Barker R A and Estrup P J 1977 *Phys. Rev. Lett.* **38** 1138
[100] Wang X W and Weber W 1987 *Phys. Rev. Lett.* **58** 1452
[101] Smith K E, Elliott G S and Kevan S D 1990 *Phys. Rev.* B **42** 5385
[102] Hulpke E and Lüdecke J 1992 *Phys. Rev. Lett.* **68** 2846
[103] Kohler B, Kuggerone P, Wilke S and Scheffler M 1995 *Phys. Rev. Lett.* **74** 1387
[104] Hoffmann F M, Persson B N J, Walter W, King D A, Hirschnagl C J and Williams G P 1994 *Phys. Rev. Lett.* **72** 1256
[105] Swamy K, Menzel A, Beer R and Bertel E 2001 *Phys. Rev. Lett.* **86** 1299
[106] Yeom H W, Takeda S, Rotenberg E, Matsuda I, Horikoshi K, Schaefer J, Lee C M, Kevan S D, Ohta T, Nagao T and Hasegawa S 1999 *Phys. Rev. Lett.* **82** 4898
[107] Nakagawa T, Boishin G I, Fujioka H, Yeom H W, Matsuda I, Takagi N, Nishijima M and Aruga T 2001 *Phys. Rev. Lett.* **86** 854
[108] Martínez-Blanco J, Joco V, Ascolani H, Tejeda A, Quirós C, Panaccione G, Balasubramanian T, Segovia P and Michel E G 2005 *Phys. Rev.* B **72** 041401(R)
[109] Bovet M, Popovic D, Clerc F, Koitzsch C, Probst U, Bucher E, Berger H, Naumovic D and Aebi P 2004 *Phys. Rev.* B **69** 125117
[110] Kevan S D 1994 *Surf. Sci.* **307** 832
[111] Damascelli A, Hussain Z and Shen Z X 2003 *Rev. Mod. Phys.* **75** 473
[112] Mannella N, Yang W L, Zhou X J, Zheng H, Mitchell J F, Zaanen J, Devereaux T P, Nagaosa N, Hussain Z and Shen Z-X 2005 *Nature* **438** 474
[113] Bostwick A, Ohta T, Seyller T, Horn K and Rotenberg E 2006 *Nat. Phys.* **3** 36
[114] Avila J, Mascaraque A, Michel E G and Asensio M C 1999 *J. Electron Spectrosc. Relat. Phenom.* **101–103** 361
[115] Avila J, Huttel Y, Le Lay G and Asensio M C 2000 *Appl. Surf. Sci.* **162/163** 48
[116] Luttinger J M 1960 *Phys. Rev.* **119** 1153
[117] Mascaraque A, Avila J, Asensio M C and Michel E G 1999 *Surf. Sci.* **433–435** 337
[118] Kidd T E, Miller T, Chou M Y and Chiang T-C 2000 *Phys. Rev. Lett.* **85** 3684